H1 restricts euchromatin-associated methylation pathways from heterochromatic encroachment

C. Jake Harris[1,2,6,#], Zhenhui Zhong[1,3,6], Lucia Ichino[1], Suhua Feng[1,4], Steven E. Jacobsen[1,4,5,#]

[1] Department of Molecular, Cell and Developmental Biology, University of California, Los Angeles, CA, USA.

[2] Present address: Department of Plant Sciences, University of Cambridge, Cambridge CB2 3EA, UK.

[3] Present address: Ministry of Education Key Laboratory for Bio-Resource and Eco-Environment, College of Life Sciences, Sichuan University, Chengdu 610065, China.

[4] Eli & Edythe Broad Center of Regenerative Medicine & Stem Cell Research, University of California, Los Angeles, Los Angeles, CA, USA.

[5] Howard Hughes Medical Institute, University of California, Los Angeles, CA, USA.

[6] These authors contributed equally.

[#] Correspondence: cjh92@cam.ac.uk and jacobsen@ucla.edu

ABSTRACT:

Silencing pathways prevent transposable element (TE) proliferation and help to maintain genome integrity through cell division. Silenced genomic regions can be classified as either euchromatic or heterochromatic, and are targeted by genetically separable epigenetic pathways. In plants, the RNA-directed DNA methylation (RdDM) pathway targets mostly euchromatic regions, while CMT DNA methyltransferases are mainly associated with heterochromatin. However, many epigenetic features - including DNA methylation patterning - are largely indistinguishable between these regions, so how the functional separation is maintained is unclear. The linker histone H1 is preferentially localized to heterochromatin and has been proposed to restrict RdDM from encroachment. To test this hypothesis, we followed RdDM genomic localization in an *h1* mutant by performing ChIP-seq on the largest subunit, NRPE1, of the central RdDM polymerase, Pol V. Loss of H1 resulted in NRPE1 enrichment predominantly in heterochromatic TEs. Increased NRPE1 binding was associated with increased chromatin accessibility in *h1*, suggesting that H1 restricts NRPE1 occupancy by compacting chromatin. However, RdDM occupancy did not impact H1 localization, demonstrating that H1 hierarchically restricts RdDM positioning. H1 mutants experience major symmetric (CG and CHG) DNA methylation gains, and by generating an *h1/nrpe1* double mutant, we demonstrate these gains are largely independent of RdDM. However, loss of NRPE1 occupancy from a subset of euchromatic regions in *h1* corresponded to loss of methylation in all sequence contexts, while at ectopically bound heterochromatic loci, NRPE1 deposition correlated with increased methylation specifically in the CHH context. Additionally, we found that H1 similarly restricts the occupancy of the methylation reader, SUVH1, and polycomb-mediated H3K27me3. Together, the results support a model whereby H1 helps maintain the exclusivity of heterochromatin by preventing encroachment from other competing pathways.

INTRODUCTION:

Eukaryotic genomes are compartmentalized into euchromatic and heterochromatin regions (Ruiz-Velasco and Zaugg, 2017). In euchromatin, nucleosomes are more accessible, while in heterochromatin nucleosomes are more compacted and restrictive to transcription. Protein coding genes are typically euchromatic, while non-coding and repetitive elements more often reside in heterochromatin. However, transposable elements, which are targeted for DNA methylation and silencing, are found in both euchromatic and heterochromatic regions of the genome (Bourque et al., 2018). The pathways responsible for deposition of methylation and silencing of TEs in these different regions are functionally and genetically distinct (Du et al., 2015).

In plants, euchromatic repetitive regions are targeted by the RNA-directed DNA methylation pathway (RdDM) (Erdmann and Picard, 2020), in which the concerted action of non-coding RNA polymerases and small RNAs direct the DNA methyltransferase, DRM2, to specific sites of the genome. Newly invading genetic elements are targeted by the 'non-canonical' RdDM pathway, and involve the action of Pol II derived small RNAs (Cuerda-Gil and Slotkin, 2016). Once established, the canonical RdDM pathway takes over, whereby small RNAs are generated by the plant-specific polymerase IV (Pol IV). In both cases, a second plant-specific polymerase, Pol V, is an essential downstream component. Pol V transcribes scaffold transcripts to which Argonaute bound small RNAs can bind through base complementarity to recruit DRM2 to direct DNA methylation (Wierzbicki et al., 2009, 2008; Zhong et al., 2014). The recruitment of Pol V to chromatin is stabilized by interaction with the DNA methylation readers SUVH2 and SUVH9 (Johnson et al., 2014). However, methylation alone is not sufficient to explain Pol V occupancy, as Pol V is restricted to the edges of long TEs and euchromatic methylated regions, despite methylation levels being high in the bodies of long TEs and in heterochromatin (Zhong et al., 2012). Therefore, additional mechanisms must exist to regulate Pol V occupancy.

Heterochromatin is targeted for DNA methylation and silencing by CMT methyltransferases (Stroud et al., 2014; Zemach et al., 2013). CMT3 and CMT2 are responsible for CHG and CHH methylation maintenance, respectively, at these regions. The CMTs form an epigenetic feedback loop with the KYP family of H3K9me2 methyltransferases, thereby maintaining high levels of repression-associated non-CG methylation and H3K9me2 at heterochromatic regions of the genome (Du et al., 2014, 2012; Li et al., 2018). As both DNA methylation and H3K9me2 are known to recruit components of the RdDM pathway (Johnson et al., 2014; Law et al., 2013), it is unclear how these regions remain functionally separated from RdDM.

The linker histone H1 associates with nucleosomes to modulate chromatin accessibility and higher order structures (Saha and Dalal, 2021). H1 binds to linker DNA as it exits from the nucleosome dyad and reduces linker DNA flexibility (Bednar et al., 2017). In plants, H1 is preferentially associated with heterochromatin, where it contributes to chromatin compaction (Bourguet et al., 2021; Choi et al., 2020; Rutowicz et al., 2019). Genetic evidence suggest that the chromatin remodeler DDM1 displaces H1 at heterochromatic TEs to facilitate access of CMT methyltransferases (Zemach et al., 2013), while

biochemical data suggests that this effect could be indirect, via DDM1s interaction with the heterochromatin associated histone variant, H2A.W (Osakabe et al., 2021). Why DDM1 grants CMTs but not RdDM access to H1-containing nucleosomes is not clear. Recent structural data shows that nucleosome bound DDM1 promotes DNA sliding (Liu et al., 2024), which may be sufficient for CMT to deposit methylation, but not for the RdDM machinery to become established. H1 also plays a key role in shaping nuclear architecture and preventing ectopic polycomb-mediated H3K27me3 deposition in telomeres (Teano et al., 2023).

Since H1 physically locks genomic DNA to the nucleosome and is preferentially associated with heterochromatin, it is a promising candidate for preventing RdDM encroachment into these regions. Recent evidence supports this hypothesis, with RdDM associated small RNAs becoming more heterochromatically enriched in *h1* knockouts (Choi et al., 2021; Papareddy et al., 2020). However, small RNAs are not a direct readout of functional RdDM activity and Pol IV dependent small RNAs are abundant in regions of the genome that do not require RdDM for methylation maintenance and that do not contain Pol V (Stroud et al., 2014). Here we directly tested whether RdDM occupancy is affected by loss of H1, by taking advantage of an endogenous Pol V antibody (which recognizes Pol V's largest subunit, NRPE1). We found that *h1* antagonizes NRPE1 occupancy throughout the genome, particularly at heterochromatic regions. This effect was not limited to RdDM, similarly impacting both the methylation reader complex component, SUVH1 (Harris et al., 2018) and polycomb-mediated H3K27me3 (Teano et al., 2023). These results suggest that H1 acts in part to restrict the function of other epigenetic pathways.

RESULTS:

To understand how H1 affects RdDM occupancy, we performed chromatin immunoprecipitation followed by sequencing (ChIP-seq) with a native antibody against NRPE1 (the largest catalytic subunit of Pol V, previously validated (Liu et al., 2018)). Two biological replicates of ChIP-seq in wild type control Col-0 and in *h1.1-1/h1.2-1* double mutant (hereafter referred to as WT and *h1,* respectively) were performed. As previously reported (Bohmdorfer et al., 2016; Liu et al., 2018; Zhong et al., 2012), NRPE1 was enriched over short TEs and at the edges of long TEs in WT (Fig. 1A-B). In the *h1* mutant, however, NRPE1 enrichment was markedly increased, with NRPE1 invading the heterochromatic bodies of long TEs (Fig. 1A-B). The negative correlation between NRPE1 enrichment and TE length observed in WT was reverted in the *h1* mutant (Fig. 1C). This suggests that mutation of *h1* facilitates the invasion of NRPE1 to more heterochromatic regions, in which long TEs tend to reside (Bourguet et al., 2021; Zemach et al., 2013). Consistent with this, NRPE1 increased more over heterochromatin associated CMT2 dependent hypo-CHH differentially methylated regions (DMRs) than at the RdDM associated DRM2 dependent CHH sites (Fig. 1D). The preferential enrichment of NRPE1 in *h1* was more pronounced at TEs that overlapped with heterochromatin associated mark, H3K9me2 (Fig. 1E). Comparing NRPE1 occupancy over TEs that had previously been classified by as either 'euchromatic' or 'heterochromatic' (based on a broad range of features and small RNA expression dynamics during embryonic development (Papareddy et al., 2020), again, we found a striking increase in NRPE1 at heterochromatic over euchromatic TEs in *h1* (Fig. 1F). From a chromosomal viewpoint, NRPE1 was preferentially enriched over pericentromeric regions in *h1*, and showed corresponding depletion from the more euchromatic chromosomal arms (Fig. 1G, Supplementary Fig. 1). Importantly, we found no evidence for increased expression of NRPE1 or other methylation pathway components known to be involved in Pol V loading or stability in the *h1* mutant (Supplementary Table 1). Together, the results indicate that H1 broadly restricts NRPE1 access to chromatin, and that this effect is more pronounced in heterochromatic regions of the genome. As H1 itself is preferentially localized to heterochromatin (see Fig. 1B,D,F) (Bourguet et al., 2021; Choi et al., 2020), this suggests that H1 directly antagonises RdDM occupancy.

One mechanism by which H1 could restrict RdDM access is by promoting chromatin compaction. Consistent with this idea and previous reports (Bourguet et al., 2021; Choi et al., 2020; He et al., 2019; Rutowicz et al., 2019), we observed increased accessibility in heterochromatic regions in *h1*, which mirrored the preferential recruitment of NRPE1 to heterochromatin (Supplementary Fig. 2AB). Loss of H1 mediated compaction in heterochromatin may be the indirect result of loss of heterochromatin associated marks such as H3K9me2. To examine this possibility, we performed H3K9me2 ChIP-seq, and although we observed some minor reductions in H3K9me2 in *h1*, the losses were not preferentially in heterochromatin where we see the majority of NRPE1 gain (Supplementary Fig. 2CD). While we cannot exclude the possibility that other heterochromatin associated marks are altered, the data suggests that H1 primarily affects the accessibility, rather than the nature of chromatin at these heterochromatic regions.

140 To determine whether the antagonistic relationship between H1 and NRPE1 is reciprocal, we performed
141 ChIP-seq using an endogenous antibody for H1, with two biological replicates in the WT and *nrpe1*
142 mutant backgrounds. H1 levels were broadly unchanged in *nrpe1* at TE regions (Fig. 2A). Similarly,
143 over NRPE1 defined peaks (where NRPE1 occupancy is strongest in WT) we observed no change in
144 H1 occupancy in *nrpe1* (Fig. 2B). The results indicate that H1 does not invade RdDM regions in the
145 *nrpe1* mutant background.
146
147 Next, we asked whether ectopic recruitment of RdDM may be sufficient to evict H1 from the genome.
148 For this, we took advantage of the ZF-DMS3 transgenic lines that we previously characterized, in which
149 zinc finger (ZF) fused DMS3 can recruit endogenous NRPE1 to >10,000 ectopic sites throughout the
150 genome, corresponding to ZF 'off-target' binding sites (Gallego-bartolome et al., 2019). With these lines,
151 we performed NRPE1 and H1 ChIP-seq in parallel. Compared to the non-transgenic control, we
152 confirmed that NRPE1 was highly enriched at these 'off-target' regions (Fig 2C). However, with the
153 same material, we observed no depletion of H1 at the ectopically bound NRPE1 sites (Fig. 2C). We
154 validated the quality of our H1 ChIPs, demonstrating antibody specificity, showing that they follow the
155 previously described profiling patterns over H2A.W associated TEs (Bourguet et al., 2021), H3K27me3
156 marked/unmarked genes (Teano et al., 2023), and that H1.2 occupancy (Teano et al., 2023) is similarly
157 enriched over our H1 peaks (Supplementary Fig. 3). To exclude the possibility that NRPE1 alone may
158 be insufficient to evict H1, but that the fully functioning RdDM pathway may be required (which
159 constitutes at least 32 described proteins acting in concert (Matzke and Mosher, 2014)), we focused on
160 the subset of ZF-DMS3 off-target sites that experience hyper-CHH methylation (Gallego-bartolome et
161 al., 2019). The gain of ectopic methylation at these regions indicates that the full RdDM pathway is
162 recruited and functions to deposit *de novo* methylation. However, even at these regions where H1 is
163 mildly enriched in WT, we saw no evidence for H1 depletion in the ZF-DMS3 transgenic lines (Fig. 2D).
164 Together, these results indicate that H1 hierarchically and non-reciprocally restricts RdDM from
165 overaccumulation in heterochromatin.
166
167 Given our observation that NRPE1 is redistributed in *h1*, we wondered whether this could help to explain
168 some of the unusual methylation defects observed in the *h1* mutant. For instance, *h1* mutants
169 experience contrasting loss and gain of DNA methylation at euchromatic and heterochromatic TEs,
170 respectively (Bourguet et al., 2021; Zemach et al., 2013). Previous explanations to account for this
171 suggested that the *h1* afforded increased accessibility of euchromatic TEs may promote increased
172 access by activation-associated chromatin modifying enzymes, which in turn antagonise DNA
173 methylation (Zemach et al., 2013). Another non-mutually exclusive scenario is that euchromatic loss
174 and heterochromatic gain of methylation is caused by the relative shift of RdDM from euchromatin to
175 heterochromatin. To directly test this possibility, we generated two independent NRPE1 CRISPR
176 knockouts in the *h1* mutant background (Supplementary Fig. 4AB), and performed whole genome
177 bisulfite sequencing (WGBS) analysis, alongside *nrpe1*, *h1* and WT controls. We confirmed *nrpe1* loss
178 of function in the independent CRISPR KO lines by plotting CHH methylation over NRPE1 associated
179 high confidence DMRs (Zhang et al., 2018), finding that CHH methylation is entirely abolished over
180 these regions in both *nrpe1/h1* lines (Supplementary Fig. 4C). By analysis of chromosome level DNA

181 methylation patterns in the different mutant backgrounds, we found that the striking pericentromeric
182 increase in CG and CHG methylation observed in *h1*, is almost entirely independent of RdDM, as it was
183 not rescued in *nrpe1/h1* (Fig. 3A, Supplementary Fig. 5). In contrast, CHH methylation was mostly
184 unaltered between the genotypes at the chromosome scale, with evidence for a slight reduction of CHH
185 in the *h1/nrpe1* double mutant as compared to *h1* alone (Fig. 3A, Supplementary Fig. 5).
186
187 Next, we compared methylation levels in euchromatic versus heterochromatic TEs. Heterochromatic
188 TEs experienced major increases in CG and CHG methylation in *h1* as previously reported (Zemach et
189 al., 2013), and these were independent of NRPE1 function, as the same increases were observed in
190 *nrpe1/h1* (Fig. 3B). CHH levels were largely unchanged at heterochromatic TEs in all mutant
191 backgrounds (Fig. 3B). At euchromatic TEs, CG and CHG methylation levels were largely unchanged
192 in *h1*, while CHH levels were markedly reduced as previously reported (Fig. 3C). CHH methylation
193 levels were further reduced in *nrpe1*, consistent with the well-established role of RdDM in maintaining
194 CHH at euchromatic TEs (Stroud et al., 2013), with the additional mutation of *h1* in *nrpe1/h1* having a
195 minimal effect (Fig. 3C). However, we noticed that the loss of CHG methylation in *nrpe1* was largely
196 rescued in the *nrpe1/h1* double mutant (Fig. 3C). This striking effect was specific to euchromatic TEs.
197 NRPE1 is therefore required for CHG methylation maintenance at euchromatic TEs and in the absence
198 of H1, loss of RdDM can be functionally compensated for by other methylation pathways. This
199 compensation is likely due to the action of CMT3 (Stroud et al., 2014; Zemach et al., 2013). The effect
200 is reminiscent of *h1*'s amelioration of methylation loss in the chromatin remodeler mutant, *ddm1*
201 (Zemach et al., 2013), and further supports a role for H1 in demarcating the boundary between
202 heterochromatic and euchromatic methylation pathways.
203
204 Calling DMRs in the mutant backgrounds, we found that *h1* hyper CHG DMRs were by far the most
205 numerous as compared to any other context (Fig. 4A). Consistent with the average methylation
206 chromosomal and TE plots, these hyper CHG DMRs were highly enriched over pericentromeric
207 heterochromatin (Fig. 4B). To gain insight into the functional context of methylation in these regions,
208 we performed overlap analysis between *h1* hyper CHG DMRs and DMRs from 96 other Arabidopsis
209 gene silencing mutants that were published previously (Stroud et al., 2013). Building similarity matrices
210 based on pairwise overlapping scores (Co-Occurrence Statistics), we observed separation of clustering
211 of mutants belonging to different functional pathways (Fig. 4C, Supplementary Fig. 6), consistent with
212 previous studies (Stroud et al., 2013; Zhang et al., 2018). The *h1* hyper CHG DMRs clustered primarily
213 with components of the CG maintenance pathway, including *met1* and *vim1/2/3* (Fig. 4D). Interestingly,
214 the *h1* hyper CHG DMRs also clustered and correlated strongly with *ddm1* hyper CHH DMRs. As
215 heterochromatic transposons are known to transition from a state of quiescence to being actively
216 targeted by RdDM in the *ddm1* mutant (Panda et al., 2016), this again suggests that H1 controls regions
217 of the genome that are susceptible to spurious RdDM targeting.
218
219 While the majority of methylation changes observed in *h1* (hyper CG and CHG) were entirely
220 independent of NRPE1, in the chromosomal plots we noted a subtle depletion of CHH methylation in

221 the *h1/nrpe1* double mutant as compared to *h1* alone (Fig. 3A), suggesting that redistribution of NRPE1
222 may have functional consequences on methylation patterning. To explicitly investigate these ectopically
223 bound loci, we compared NRPE1 enrichment in WT versus *h1* and identified 15,075 peaks that have
224 significantly higher NRPE1 signal in the *h1* mutant. At these regions, CG and CHG methylation changes
225 broadly mirrored that of heterochromatic TEs, again supporting the notion that NRPE1 primarily
226 redistributes to heterochromatic regions of the genome in *h1* (Fig. 5A, Supplementary Fig. 7A).
227 However, we also observed a significant depletion of CHH methylation at these regions in the *nrpe1/h1*
228 double mutant, as compared to either the *h1* and *nrpe1* alone, which was not observed when looking
229 at heterochromatic TEs as a whole (compare Fig. 5A to Fig. 3B). This indicates that NRPE1 facilitates
230 active deposition of CHH methylation at these newly bound locations. Reciprocally, we asked how
231 methylation changes at regions of the genome that lose NRPE1 in *h1* (1,859 peaks), and we found that
232 methylation levels are significantly depleted in all three contexts (CG, CHG and CHH) in the *h1*, *nrpe1*
233 and *nrpe1/h1* double mutant backgrounds (Fig. 5B, Supplementary Fig. 7B and 8). The mirrored loss
234 and gain of methylation with changes in NRPE1 occupancy indicates that NRPE1 redistribution in *h1*
235 directly impacts methylation patterning *in cis*.
236
237 The results thus far support a model whereby H1 prevents RdDM encroachment into heterochromatin.
238 As H1 likely restricts access by reducing chromatin accessibility at these regions, we reasoned that this
239 effect would not be RdDM specific and could affect other machinery in a similar manner. The SUVH1
240 methyl binding protein directly binds CHH methylation *in vitro*, yet shows strong preferential recruitment
241 to RdDM over CMT dependent sites *in vivo* (Harris et al., 2018). Along with SUVH3, SUVH1 functions
242 to protect the expression of genes residing nearby to RdDM targeted transposable elements by
243 recruiting DNAJ1/2 transcriptional activators. We therefore wondered whether the SUVH1's occupancy
244 might also be affected by H1. To test this, we performed ChIP-seq on SUVH1-3xFLAG in an *h1* mutant
245 background (Fig. 6A). As with NRPE1, SUVH1 was generally enriched throughout the genome in *h1*,
246 but the effect was strongest over heterochromatin (long TEs, *cmt2*-dependent hypo-CHH DMRs, and
247 heterochromatic TEs, Fig. 6B). At the transcript level, we saw no evidence that SUVH1 or related
248 complex components are upregulated in the *h1* mutant background (Supplementary Table 1), however,
249 we cannot rule out the possibility that the SUVH1-3xFLAG transgene is expressed more highly in *h1*.
250 Teano et al recently showed that polycomb dependent H3K27me3 is redistributed in *h1*. We compared
251 sites that gain NRPE1 to sites that gain H3K27me3 in *h1*, finding a statistically significant overlap (2.4
252 fold enrichment over expected, hypergeometric test p-value $2.1e^{-71}$). Reciprocally, sites that lose
253 NRPE1 were significantly enriched for overlap with H3K27me3 loss regions (1.6 fold over expected,
254 hypergeometric test p-value $1.4e^{-4}$). This indicates that RdDM and H3K27me3 patterning are similarly
255 modulated by H1. To directly test this, we reanalysed the H3K27me3 ChIP-seq data from Teano et al.,
256 finding coincident enrichment and depletion of H3K27me3 at sites that gain and lose NRPE1 in *h1* (Fig
257 6E). Therefore, H1 acts in a non-RdDM specific manner, to prevent euchromatic machinery from
258 heterochromatic encroachment, likely through promoting nucleosome compaction and restricting
259 access to chromatin.

260 **DISCUSSION:**

261 Here we show that loss of H1 results in redistribution of RdDM from euchromatic to heterochromatic
262 regions, consistent with recent findings from small RNA data (Choi et al., 2021; Papareddy et al., 2020).
263 This ectopic accumulation results in modest but detectable NRPE1-dependent methylation, and it would
264 be interesting to determine whether Pol V transcript production and DRM2 methyltransferase
265 recruitment occurs in a similar manner to euchromatin in these regions. It is important to note that
266 NRPE1 binding was generally increased in the *h1* mutant (both euchromatin and heterochromatin),
267 consistent with H1's widespread occupancy through the genome, but that the effect was strongest in
268 heterochromatin where H1 shows maximal enrichment (Bourguet et al., 2021; Choi et al., 2020;
269 Rutowicz et al., 2019). The antagonism of RdDM by H1 is non-reciprocal, as H1 levels were not affected
270 by RdDM loss, or artificial gain at ectopic regions of the genome. H1-mediated restriction could be in
271 part due to its structural capacity to reduce linker DNA flexibility (Bednar et al., 2017), thereby reducing
272 polymerase access to unwind and interact with genomic DNA. Pol V requires the DDR complex for
273 efficient association with chromatin (Wongpalee et al., 2019), so the presence of H1 could present an
274 additional barrier to this complex. Mammalian H1 has been shown to compact chromatin in part through
275 the phase separating property of its highly charged intrinsically disordered domain (Gibson et al., 2019).
276 Consistent with this, very recent work in Arabidopsis showed that H1 induced phase separation and
277 that this capacity was essential for the stability of heterochromatic nuclear foci (He et al., 2024).
278 Therefore, another possibility is that high H1 occupancy creates a biophysical environment that
279 excludes Pol V and related complexes. Our data together with the observed heterochromatic
280 encroachment of Pol IV dependent small RNAs in *h1* (Choi et al., 2021; Papareddy et al., 2020), along
281 with H1's recently described role in preventing spurious antisense transcription at protein coding genes
282 (Choi et al., 2020), support a polymerase indiscriminate model for H1's antagonism.
283
284 Small RNAs are relatively abundant in heterochromatin, despite Pol IV and RdDM being dispensable
285 for methylation in these regions (Stroud et al., 2014). This suggests that Pol IV occupies
286 heterochromatin, but that RdDM is either impotent for methylation deposition or acts redundantly with
287 the CMT/KYP pathway. Here we detect NRPE1-dependent methylation at heterochromatic loci in *h1,*
288 and combined with the finding that Pol V does not appreciably enter these regions in WT, suggests that
289 H1 prevents RdDM from fully mobilizing in these regions by blocking Pol V. Recent evidence suggests
290 that Pol V can be directly recruited by small RNAs to establish methylation (Sigman et al., 2021), and
291 therefore mechanisms that preclude Pol V recruitment to heterochromatin would be particularly crucial
292 in preventing redundant RdDM activity at regions where methylation has already been established.
293
294 In *Arabidopsis thaliana*, RdDM targets evolutionarily young transposable elements (Zhong et al., 2012).
295 H1 therefore helps to improve the efficiency of RdDM by focusing it upon TEs with the greatest potential
296 to mobilize. As transposons age, they eventually become targeted by CMTs. How this transition occurs
297 is unclear, but our results indicate a potential role for progressive accumulation of H1 in this process.
298 Interestingly in tomato, CMTs rather than RdDM target the evolutionarily younger elements (Wang and
299 Baulcombe, 2020), therefore it will be important to determine whether H1 plays a similar role in

maintaining the barrier between methylation pathways in this context. Recent work has shown that H1 co-operates with H2A.W to promote compaction at heterochromatic regions (Bourguet et al., 2021). However, H2A.W was found to antagonize rather than promote H1 deposition at heterochromatin. Therefore, the features that drive H1 to preferentially incorporate into heterochromatin are yet to be discovered.

305 # METHODS:

306 **Plant materials and growth conditions:**

307 *Arabidopsis thaliana* plants in this study were Col-0 ecotype and were grown under 16h light: 8h dark
308 condition (on soil), or under constant light (on plates). The following plant materials were used: wild-
309 type (WT, non-transgenic), *h1* (double homozygous mutant consisting of, *h1.1-1* [SALK_128430] and
310 *h1.2–1* [GABI_406H11], originally described by (Zemach et al., 2013)), *nrpe1* (*nrpe1-11*
311 [SALK_029919]), ZF-DMS3 (this is a homozygous transgenic line containing the pEG302-DMS3-
312 3xFLAG-ZF construct in Col-0 WT, originally described by (Gallego-bartolome et al., 2019)), SUVH1-
313 3xFLAG in *suvh1* (this is a complementing homozygous transgenic line containing the pEG302-
314 gSUVH1-3xFLAG construct in *suvh1-1*, originally described by (Harris et al., 2018)), SUVH1-3xFLAG
315 in *h1* (this line was generated for this work, by transforming the same pEG302-gSUVH1-3xFLAG
316 construct into the *h1.1-1* [SALK_128430] and *h1.2–1* [GABI_406H11] double mutant background),
317 and the *h1*/*nrpe1* CRISPR lines (described below).

318

319 **Generation of CRISPR lines:**

320 Two independent NRPE1 knockout lines were generated in the background of *h1* (*h1.1-1 h1.2-1* double,
321 see above), designated as *h1/nrpe1* cKO_49 and *h1/nrpe1* cKO_63. The lines were generated using
322 the previously published pYAO::hSpCas9 system (Yan et al., 2015) as described by (Ichino et al., 2021).
323 Briefly, the two guides (ATTCTTGACGGAGAGATTGT, and TCTGGCACTGACAAACAGTT) targeting
324 hSpCas9 to NRPE1 (AT2G40030) exons were sequentially cloned in the SpeI linearized
325 pYAO::hSpCas9 construct by In-Fusion (Takara, cat #639650). The final vector was electroporated into
326 AGL0 agrobacteria and transformed in *h1* mutant plants by agrobacterium-mediated floral dipping. T1
327 plants were selected on ½ MS agar plates with hygromycin B and were PCR genotyped to identify
328 plants with deletions spanning the guide region. Selected lines were taken to T2 and genotyped to
329 identify those that had segregated out the pYAO::hSpCas9 transgene. Cas9 negative plants that were
330 homozygous for an NRPE1 deletion (*h1/nrpe1* cKO_49) or an indel-induced frameshift to premature
331 stop codon (*h1/nrpe1* cKO_63) were confirmed in the T3 generation (see Supplementary Fig. 4).

332

333 **Chromatin immunoprecipitation sequencing (ChIP-seq) and western blot:**

334 All the material for ChIP used in this paper were from pooled 10-12 days old seedlings grown on
335 Murashinge and Skoog agar plates (1/2X MS, 1.5% agar, pH5.7). The ChIP protocol used has been
336 previously described (Ichino et al., 2021; Villar and Kohler, 2018), with minor modifications. Briefly, 2-
337 4g of seedling tissue was used for each sample. Samples were ground in liquid nitrogen and crosslinked
338 for 10 or 12 minutes at room temperature in Nuclei Isolation buffer (50mM Hepes pH8, 1M sucrose,
339 5mM KCl, 5mM MgCl2, 0.6% triton X-100, 0.4mM PMSF, 5mM benzamidine hydrochloride, cOmplete
340 EDTA-free Protease Inhibitor Cocktail (Roche)) containing 1% formaldehyde. The crosslinking
341 reactions were stopped with 125mM glycine by incubation at room temperature for 10 minutes.
342 Crosslinked nuclei were filtered through one layer of miracloth, washed with Extraction Buffer 2,
343 centrifuged through a layer of Extraction Buffer 3 and lysed with Nuclei lysis buffer (buffer compositions
344 are described in the published protocol (Villar and Kohler, 2018)). Chromatin was sheared using a

345 Bioruptor Plus (Diagenode) (20 cycles of 30 seconds on and 30 seconds off) and immunoprecipitated
346 overnight at 4°C with antibody. anti-NRPE1 (endogenous antibody, described in (Liu et al., 2018)), anti-
347 H1 (Agrisera, AS11 1801), anti-H3K9me2 (abcam, 1220), anti-H3 (abcam, 1791), anti-FLAG (for both
348 the SUVH1-3xFLAG and the DMS3-ZF ChIPs, we used Anti-FLAG M2 (Sigma, F1804)). 25µl each of
349 Protein A and Protein G magnetic Dynabeads (Invitrogen) were added to each sample and incubated
350 for 2 more hours at 4°C. The immunoprecipitated chromatin was washed with Low Salt (2X), High Salt,
351 LiCl and TE buffers, for 5 minutes each at 4°C (buffer compositions are described in the published
352 protocol (Villar and Kohler, 2018)) and eluted twice with 250µl of elution buffer (1% SDS and 0.1M
353 NaHCO3) in a thermomixer at 65°C and 1000 rpm, 20 minutes for each elution. Reverse crosslinking
354 was performed overnight at 65°C in 0.2M NaCl, and proteins were degraded by proteinase K treatment
355 at 45°C for 5h. The DNA fragments were purified using phenol:chloroform and ethanol precipitated
356 overnight at -20°C. Libraries were prepared using the Ovation Ultralow System V2 kit (NuGEN,
357 0344NB-A01) following the manufacturer's instructions, with 15 cycles of PCR. Libraries were
358 sequenced on a HiSeq 4000 or NovaSeq 6000 instrument (Illumina) using either single- or paired-end
359 50bp reads.
360
361 For the western blot shown in Supplementary Fig. 3A, 100ul of sheared chromatin was used as the
362 input material for SDS-PAGE (as previously described (Harris et al., 2016)), using the anti-NRPE1 and
363 anti-H1 antibodies described above.
364
365 **ChIP-seq data analysis:**
366 ChIP-seq data were aligned to the TAIR10 reference genome with Bowtie2 (v2.1.0) (Langmead and
367 Salzberg, 2012) allowing only uniquely mapping reads with zero mismatch. Duplicated reads were
368 removed by Samtools. ChIP-seq peaks were called by MACS2 (v2.1.1) and annotated with ChIPseeker
369 (Yu et al., 2015). Bigwig tracks were generated using the deepTools (v2.5.1) (Ramírez et al., 2016)
370 bamCompare function, with samples scaled by mapped read count (--scaleFactorsMethod readCount)
371 prior to $\log_2$ ratio or subtraction normalisation against corresponding input (Liu et al., 2018) or control
372 samples. These tracks were used to generate metaplots using the computeMatrix and plotProfile /
373 plotHeatmap functions in deepTools. Differential peaks were called by bdgdiff function in MACS2
374 (Zhang et al., 2008).
375
376 **Whole-genome bisulfite sequencing (BS-seq) library preparation:**
377 Whole genome bisulfite sequencing libraries were generated as previously described (Harris et al.,
378 2016), with minor modifications. The DNeasy Plant Mini Kit (Qiagen #69104) was used to isolate
379 genomic DNA. 150µg of genomic DNA was used as input, a Covais S2 instrument was used for
380 shearing (2 minutes), the Epitect Kit (QIAGEN #59104) was used for bisulfite conversion, and the
381 Ultralow Methyl Kit (NuGEN) was used for library preparation and paired-end libraries were sequenced
382 on a NovaSeq 6000 instrument.
383
384 **Whole-genome bisulfite sequencing (BS-seq) data analysis:**

Previously published whole-genome bisulfite sequencing data for mutants and wild type were reanalyzed from previous paper (Stroud et al., 2013). Briefly, Trim_galore (http://www.bioinformatics.babraham.ac.uk/projects/trim_galore/) was used to trim adapters. BS-seq reads were aligned to TAIR10 reference genome by BSMAP (v2.90) and allowed 2 mismatches and 1 best hit (-v 2 -w 1) (Xi and Li, 2009). Reads with three or more consecutive CHH sites were considered as unconverted reads and filtered. DNA methylation levels were defined as #mC/ (#mC + #unmC). DMR overlapping analysis were conducted by mergePeaks (-d 100) of Homer (Heinz et al., 2010) with WGBS data published previously (Stroud et al., 2013). The estimated conversion rates for all WGBS libraries are provided in Supplementary Table 2**.**

Data and code availability:

Data supporting the findings of this work are available within the paper and its Supplementary Information files. All high-throughput sequencing data generated in this study are accessible at NCBI's Gene Expression Omnibus (GEO) via GEO Series accession number GSE225480 (https://www.ncbi.nlm.nih.gov/geo/query/acc.cgi?acc=GSE225480). The pipelines and codes for downstream analysis are available on GitHub (https://github.com/Zhenhuiz/H1-restricts-euchromatin-associated-methylation-pathways-from-heterochromatic-encroachment). The bed files used to generate to plots are supplied in Supplementary Table 3.

ACKNOWLEDGEMENTS:

We thank Mahnaz Akhavan for support with high-throughput sequencing at the UCLA Broad Stem Cell Research Center BioSequencing Core Facility. C.J.H is supported by a Royal Society University Research Fellowship (URF\R1\201016). This work was supported by NIH R35 GM130272 to S.E.J.. S.E.J is an Investigator of the Howard Hughes Medical Institute.

AUTHOR CONTRIBUTIONS:

C.J.H. and S.E.J. designed the research. C.J.H., Z.Z. and S.E.J. wrote the manuscript. L.I. helped to isolate the *h1/nrpe1* CRISPR knockout lines. S.F. generated the WGBS libraries from genomic DNA. C.J.H. performed all other experiments. Z.Z. and C.J.H. performed the bioinformatic analyses.

414 **REFERENCES:**

415 Bednar J, Garcia-Saez I, Boopathi R, Cutter AR, Papai G, Reymer A, Syed SH, Lone IN, Tonchev O,
416 Crucifix C, Menoni H, Papin C, Skoufias DA, Kurumizaka H, Lavery R, Hamiche A, Hayes JJ,
417 Schultz P, Angelov D, Petosa C, Dimitrov S. 2017. Structure and Dynamics of a 197 bp
418 Nucleosome in Complex with Linker Histone H1. *Mol Cell* **66**:384-397.e8.
419 doi:10.1016/j.molcel.2017.04.012

420 Bohmdorfer G, Sethuraman S, Jordan Rowley M, Krzyszton M, Hafiz Rothi M, Bouzit L, Wierzbicki AT.
421 2016. Long non-coding RNA produced by RNA polymerase V determines boundaries of
422 heterochromatin. *Elife* **5**:1–24. doi:10.7554/eLife.19092

423 Bourguet P, Picard CL, Yelagandula R, Pélissier T, Lorković ZJ, Feng S, Pouch-Pélissier MN,
424 Schmücker A, Jacobsen SE, Berger F, Mathieu O. 2021. The histone variant H2A.W and linker
425 histone H1 co-regulate heterochromatin accessibility and DNA methylation. *Nat Commun* **12**:1–
426 12. doi:10.1038/s41467-021-22993-5

427 Bourque G, Burns KH, Gehring M, Gorbunova V, Seluanov A, Hammell M, Imbeault M, Izsvák Z, Levin
428 HL, Macfarlan TS, Mager DL, Feschotte C. 2018. Ten things you should know about transposable
429 elements 06 Biological Sciences 0604 Genetics. *Genome Biol* **19**:1–12. doi:10.1186/s13059-018-
430 1577-z

431 Choi J, Lyons DB, Kim MY, Moore JD, Zilberman D. 2020. DNA Methylation and Histone H1 Jointly
432 Repress Transposable Elements and Aberrant Intragenic Transcripts. *Mol Cell* **77**:310-323.e7.
433 doi:10.1016/j.molcel.2019.10.011

434 Choi J, Lyons DB, Zilberman D. 2021. Histone H1 prevents non-CG methylation-mediated small RNA
435 biogenesis in Arabidopsis heterochromatin. *Elife* **10**:1–24. doi:10.7554/eLife.72676

436 Cuerda-Gil D, Slotkin RK. 2016. Non-canonical RNA-directed DNA methylation. *Nat Plants* **2**.
437 doi:10.1038/nplants.2016.163

438 Du J, Johnson LM, Groth M, Feng S, Hale CJ, Li S, Vashisht AA, Gallego-Bartolome J, Wohlschlegel
439 JA, Patel DJ, Jacobsen SE. 2014. Mechanism of DNA methylation-directed histone methylation
440 by KRYPTONITE. *Mol Cell* **55**:495–504. doi:10.1016/j.molcel.2014.06.009

441 Du J, Johnson LM, Jacobsen SE, Patel DJ. 2015. DNA methylation pathways and their crosstalk with
442 histone methylation. *Nat Rev Mol Cell Biol* **16**:519–532. doi:10.1038/nrm4043

443 Du J, Zhong X, Bernatavichute Y V, Stroud H, Feng S, Caro E, Vashisht AA, Terragni J, Chin HG, Tu
444 A, Hetzel J, Wohlschlegel JA, Pradhan S, Patel DJ, Jacobsen SE. 2012. Dual binding of
445 chromomethylase domains to H3K9me2-containing nucleosomes directs DNA methylation in
446 plants. *Cell* **151**:167–80. doi:10.1016/j.cell.2012.07.034

447 Erdmann RM, Picard CL. 2020. RNA-directed DNA Methylation, PLoS Genetics.
448 doi:10.1371/journal.pgen.1009034

449 Gallego-bartolome J, Liu W, Kuo PH, Feng S, Ghoshal B, Gardiner J, Park SY, Chory J, Jacobsen SE,
450 Liu W, Kuo PH, Feng S, Ghoshal B, Gardiner J, Zhao JM, Park SY, Chory J, Jacobsen SE. 2019.
451 Co-targeting RNA Polymerases IV and V Promotes and V Promotes Efficient De Novo DNA
452 Methylation in Arabidopsis. *Cell* **176**:1–15. doi:10.1016/j.cell.2019.01.029

453 Gibson BA, Doolittle LK, Schneider MWG, Jensen LE, Gamarra N, Henry L, Gerlich DW, Redding S,

454 Rosen MK. 2019. Organization of Chromatin by Intrinsic and Regulated Phase Separation. *Cell*
455 **179**:470-484.e21. doi:10.1016/j.cell.2019.08.037
456 Harris CJ, Husmann D, Liu W, Kasmi F El, Wang H, Papikian A, Pastor WA, Moissiard G, Vashisht AA,
457 Dangl JL, Wohlschlegel JA, Jacobsen SE. 2016. Arabidopsis AtMORC4 and AtMORC7 Form
458 Nuclear Bodies and Repress a Large Number of Protein-Coding Genes. *PLOS Genet*
459 **12**:e1005998. doi:10.1371/journal.pgen.1005998
460 Harris CJ, Scheibe M, Wongpalee SP, Liu W, Zhong Z, Yen L, Barshop WD, Rayatpisheh S, Du J,
461 Rothbart SB, Butter F, Jacobsen SE. 2018. A DNA methylation reader complex that enhances
462 gene transcription. *Science* **362**:1182–1186.
463 He S, Vickers M, Zhang J, Feng X. 2019. Natural depletion of histone H1 in sex cells causes DNA
464 demethylation, heterochromatin decondensation and transposon activation. *Elife* **8**:1–23.
465 doi:10.7554/ELIFE.42530
466 He S, Yu Y, Wang L, Zhang J, Bai Z, Li G, Li P, Feng X. 2024. Linker histone H1 drives heterochromatin
467 condensation via phase separation in Arabidopsis. *Plant Cell*. doi:10.1093/plcell/koae034
468 Heinz S, Benner C, Spann N, Bertolino E, Lin YC, Laslo P, Cheng JX, Murre C, Singh H, Glass CK.
469 2010. Simple Combinations of Lineage-Determining Transcription Factors Prime cis-Regulatory
470 Elements Required for Macrophage and B Cell Identities. *Mol Cell* **38**:576–589.
471 doi:10.1016/j.molcel.2010.05.004
472 Ichino L, Boone BA, Strauskulage L, Harris CJ, Kaur G, Gladstone MA, Tan M, Feng S, Jami-alahmadi
473 Y, Duttke SH. 2021. MBD5 and MBD6 couple DNA methylation to gene silencing through the J-
474 domain protein SILENZIO. *Science (80-)* **1439**:1434–1439.
475 Johnson LM, Du J, Hale CJ, Bischof S, Feng S, Chodavarapu RK, Zhong X, Marson G, Pellegrini M,
476 Segal DJ, Patel DJ, Jacobsen SE. 2014. SRA- and SET-domain-containing proteins link RNA
477 polymerase V occupancy to DNA methylation. *Nature* **507**:124–128. doi:10.1038/nature12931
478 Langmead B, Salzberg SL. 2012. Fast gapped-read alignment with Bowtie 2. *Nat Methods* **9**:357–359.
479 doi:10.1038/nmeth.1923
480 Law J a, Du J, Hale CJ, Feng S, Krajewski K, Palanca AMS, Strahl BD, Patel DJ, Jacobsen SE. 2013.
481 Polymerase IV occupancy at RNA-directed DNA methylation sites requires SHH1. *Nature*
482 **498**:385–389. doi:10.1038/nature12178
483 Li X, Harris CJ, Zhong Z, Chen W, Liu R, Jia B, Wang Z, Li S, Jacobsen SE, Du J. 2018. Mechanistic
484 insights into plant SUVH family H3K9 methyltransferases and their binding to context-biased non-
485 CG DNA methylation. *PNAS* 1–10. doi:10.1073/pnas.1809841115
486 Liu W, Duttke SH, Hetzel J, Groth M, Feng S, Gallego-Bartolome J, Zhong Z, Kuo HY, Wang Z, Zhai J,
487 Chory J, Jacobsen SE. 2018. RNA-directed DNA methylation involves co-transcriptional small-
488 RNA-guided slicing of polymerase v transcripts in Arabidopsis. *Nat Plants* **4**:181–188.
489 doi:10.1038/s41477-017-0100-y
490 Liu Y, Zhang Z, Hu H, Chen W, Zhang F, Wang Q, Wang C, Yan K, Du J. 2024. Molecular basis of
491 chromatin remodelling by DDM1 involved in plant DNA methylation. *Nat Plants*.
492 doi:10.1038/s41477-024-01640-z
493 Matzke M a., Mosher R a. 2014. RNA-directed DNA methylation: an epigenetic pathway of increasing

494 complexity. *Nat Rev Genet* **15**:394–408. doi:10.1038/nrg3683
495 Osakabe A, Jamge B, Axelsson E, Montgomery SA, Akimcheva S, Kuehn AL, Pisupati R, Lorković ZJ,
496 Yelagandula R, Kakutani T, Berger F. 2021. The chromatin remodeler DDM1 prevents transposon
497 mobility through deposition of histone variant H2A.W. *Nat Cell Biol* **23**:391–400.
498 doi:10.1038/s41556-021-00658-1
499 Panda K, Ji L, Neumann DA, Daron J, Schmitz RJ, Slotkin RK. 2016. Full-length autonomous
500 transposable elements are preferentially targeted by expression-dependent forms of RNA-
501 directed DNA methylation. *Genome Biol* **17**:170. doi:10.1186/s13059-016-1032-y
502 Papareddy RK, Páldi K, Paulraj S, Kao P, Lutzmayer S, Nodine MD. 2020. Chromatin regulates
503 expression of small RNAs to help maintain transposon methylome homeostasis in Arabidopsis.
504 *Genome Biol* **21**:251. doi:10.1186/s13059-020-02163-4
505 Ramírez F, Ryan DP, Grüning B, Bhardwaj V, Kilpert F, Richter AS, Heyne S, Dündar F, Manke T.
506 2016. deepTools2: a next generation web server for deep-sequencing data analysis. *Nucleic Acids*
507 *Res* **44**:W160–W165. doi:10.1093/nar/gkw257
508 Ruiz-Velasco M, Zaugg JB. 2017. Structure meets function: How chromatin organisation conveys
509 functionality. *Curr Opin Syst Biol* **1**:129–136. doi:10.1016/j.coisb.2017.01.003
510 Rutowicz K, Lirski M, Mermaz B, Teano G, Schubert J, Mestiri I, Kroteń MA, Fabrice TN, Fritz S, Grob
511 S, Ringli C, Cherkezyan L, Barneche F, Jerzmanowski A, Baroux C. 2019. Linker histones are
512 fine-scale chromatin architects modulating developmental decisions in Arabidopsis. *Genome Biol*
513 **20**:1–22. doi:10.1186/s13059-019-1767-3
514 Saha A, Dalal Y. 2021. A glitch in the snitch: The role of linker histone H1 in shaping the epigenome in
515 normal and diseased cells. *Open Biol* **11**. doi:10.1098/rsob.210124
516 Sigman MJ, Panda K, Kirchner R, McLain LL, Payne H, Peasari JR, Husbands AY, Slotkin RK, McCue
517 AD. 2021. An siRNA-guided ARGONAUTE protein directs RNA polymerase V to initiate DNA
518 methylation. *Nat Plants* **7**:1461–1474. doi:10.1038/s41477-021-01008-7
519 Stroud H, Do T, Du J, Zhong X, Feng S, Johnson L, Patel DJ, Jacobsen SE. 2014. Non-CG methylation
520 patterns shape the epigenetic landscape in Arabidopsis. *Nat Struct Mol Biol* **21**:64–72.
521 doi:10.1038/nsmb.2735
522 Stroud H, Greenberg MVC, Feng S, Bernatavichute Y V, Jacobsen SE. 2013. Comprehensive Analysis
523 of Silencing Mutants Reveals Complex Regulation of the Arabidopsis Methylome. *Cell* **152**:352–
524 364. doi:10.1016/j.cell.2012.10.054
525 Teano G, Concia L, Wolff L, Carron L, Biocanin I, Adamusová K, Fojtová M, Bourge M, Kramdi A, Colot
526 V, Grossniklaus U, Bowler C, Baroux C, Carbone A, Probst A V., Schrumpfová PP, Fajkus J,
527 Amiard S, Grob S, Bourbousse C, Barneche F. 2023. Histone H1 protects telomeric repeats from
528 H3K27me3 invasion in Arabidopsis. *Cell Rep* **42**. doi:10.1016/j.celrep.2023.112894
529 Villar CBR, Kohler C. 2018. Plant Chromatin immunoprecipitation. *Methods Mol Biol* **1839**:65–75.
530 doi:10.1007/978-1-4939-8685-9_7
531 Wang Z, Baulcombe DC. 2020. Transposon age and non-CG methylation. *Nat Commun* **11**:1–9.
532 doi:10.1038/s41467-020-14995-6
533 Wierzbicki AT, Haag JR, Pikaard CS. 2008. Noncoding Transcription by RNA Polymerase Pol IVb/Pol

534 V Mediates Transcriptional Silencing of Overlapping and Adjacent Genes. *Cell* **135**:635–648.
535 doi:10.1016/j.cell.2008.09.035
536 Wierzbicki AT, Ream TS, Haag JR, Pikaard CS. 2009. RNA polymerase V transcription guides
537 ARGONAUTE4 to chromatin. *Nat Genet* **41**:630–4. doi:10.1038/ng.365
538 Wongpalee SP, Liu S, Gallego-Bartolomé J, Leitner A, Aebersold R, Liu W, Yen L, Nohales MA, Kuo
539 PH, Vashisht AA, Wohlschlegel JA, Feng S, Kay SA, Zhou ZH, Jacobsen SE. 2019. CryoEM
540 structures of Arabidopsis DDR complexes involved in RNA-directed DNA methylation. *Nat*
541 *Commun* **10**:1–12. doi:10.1038/s41467-019-11759-9
542 Xi Y, Li W. 2009. BSMAP: Whole genome bisulfite sequence MAPping program. *BMC Bioinformatics*
543 **10**:1–9. doi:10.1186/1471-2105-10-232
544 Yan L, Wei S, Wu Y, Hu R, Li H, Yang W, Xie Q. 2015. High-Efficiency Genome Editing in Arabidopsis
545 Using YAO Promoter-Driven CRISPR/Cas9 System. *Mol Plant* **8**:1820–1823.
546 doi:10.1016/j.molp.2015.10.004
547 Yu G, Wang LG, He QY. 2015. ChIP seeker: An R/Bioconductor package for ChIP peak annotation,
548 comparison and visualization. *Bioinformatics* **31**:2382–2383. doi:10.1093/bioinformatics/btv145
549 Zemach A, Kim MY, Hsieh P-H, Coleman-Derr D, Eshed-Williams L, Thao K, Harmer SL, Zilberman D.
550 2013. The Arabidopsis nucleosome remodeler DDM1 allows DNA methyltransferases to access
551 H1-containing heterochromatin. *Cell* **153**:193–205. doi:10.1016/j.cell.2013.02.033
552 Zhang Y, Harris CJ, Liu Q, Liu W, Ausin I, Long Y, Xiao L, Feng L, Chen Xu, Xie Y, Chen Xinyuan,
553 Zhan L, Feng S, Li JJ, Wang H, Zhai J, Jacobsen SE. 2018. Large-scale comparative epigenomics
554 reveals hierarchical regulation of non-CG methylation in Arabidopsis. *Proc Natl Acad Sci*
555 201716300. doi:10.1073/pnas.1716300115
556 Zhang Y, Liu T, Meyer CA, Eeckhoute J, Johnson DS, Bernstein BE, Nussbaum C, Myers RM, Brown
557 M, Li W, Shirley XS. 2008. Model-based analysis of ChIP-Seq (MACS). *Genome Biol* **9**.
558 doi:10.1186/gb-2008-9-9-r137
559 Zhong X, Du J, Hale CJ, Gallego-Bartolome J, Feng S, Vashisht AA, Chory J, Wohlschlegel JA, Patel
560 DJ, Jacobsen SE. 2014. Molecular Mechanism of Action of Plant DRM De Novo DNA
561 Methyltransferases. *Cell* **157**:1050–1060. doi:10.1016/j.cell.2014.03.056
562 Zhong X, Hale CJ, Law JA, Johnson LM, Feng S, Tu A, Jacobsen SE. 2012. DDR complex facilitates
563 global association of RNA polymerase V to promoters and evolutionarily young transposons. *Nat*
564 *Struct Mol Biol* **19**:870–5. doi:10.1038/nsmb.2354
565

FIGURES:

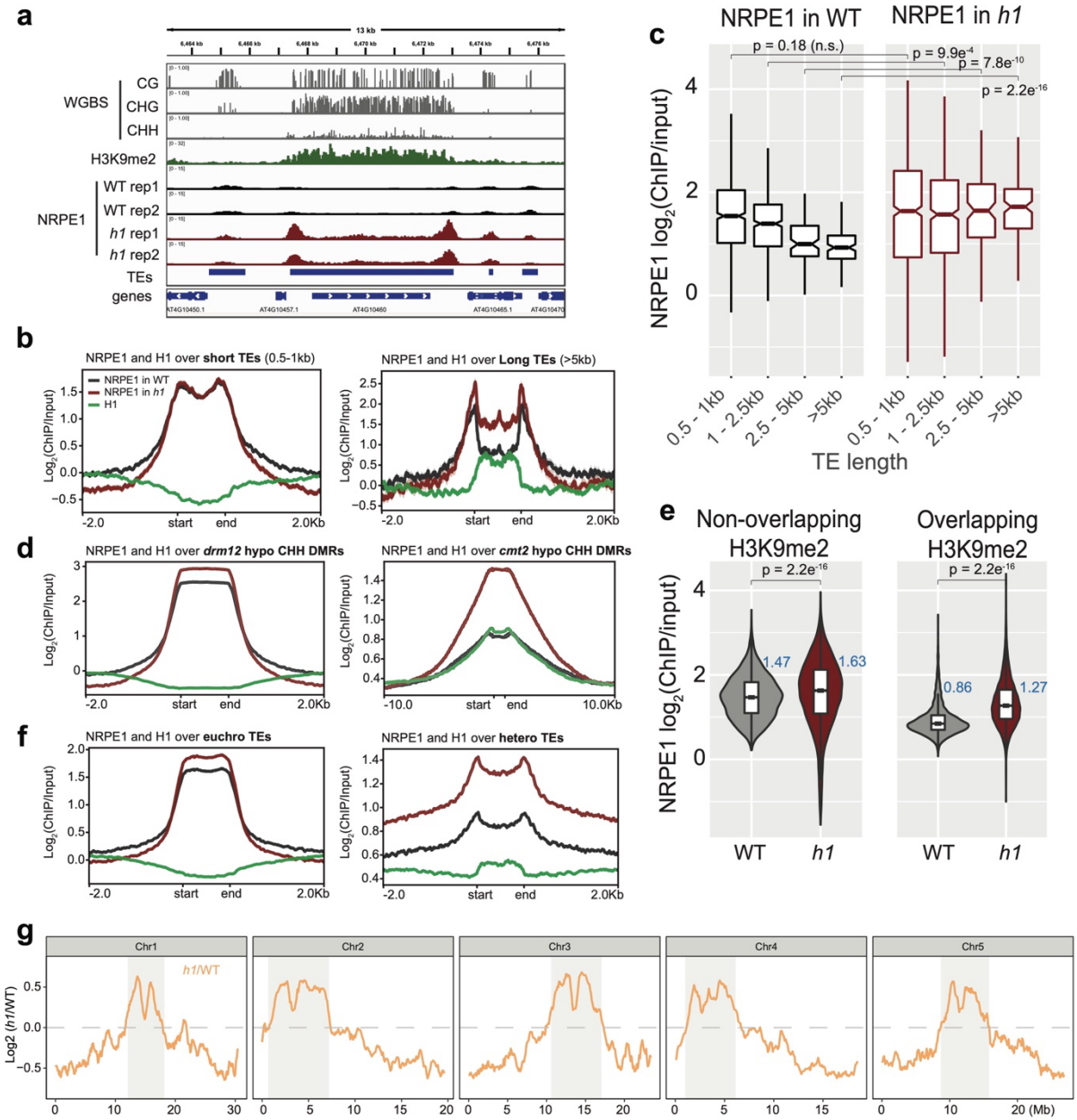

Figure 1 - NRPE1 accumulates in heterochromatin in an *h1* mutant background: A) Genome browser image showing increased NRPE1 enrichment in *h1* over heterochromatic (long, H3K9me2 enriched) and not euchromatic (short, not H3K9me2 enriched) TEs. B) metaplot showing ChIP-seq enrichment of NRPE1 in WT vs. *h1*, and H1 occupancy in WT for reference (data from GSE122394), at short vs. long TEs. C) boxplot showing association between NRPE1 and TE length in WT and *h1*. wilcoxon rank sum test p-values indicated. D) As in B) for *drm12* vs. *cmt2* hypo CHH DMRs. E) Violin plot inlaid with boxplot showing enrichment of NRPE1 at TEs that overlap with H3K9me2 peaks, vs. TEs that do not, in WT vs. *h1*. Boxplot medians are shown in blue. Wilcoxon rank sum test p-values indicated. F) as in B) at euchromatic vs. heterochromatic TEs. G) Chromosomal plots showing NRPE1 enrichment in *h1* as compared to WT, with pericentromeric regions denoted in grey.

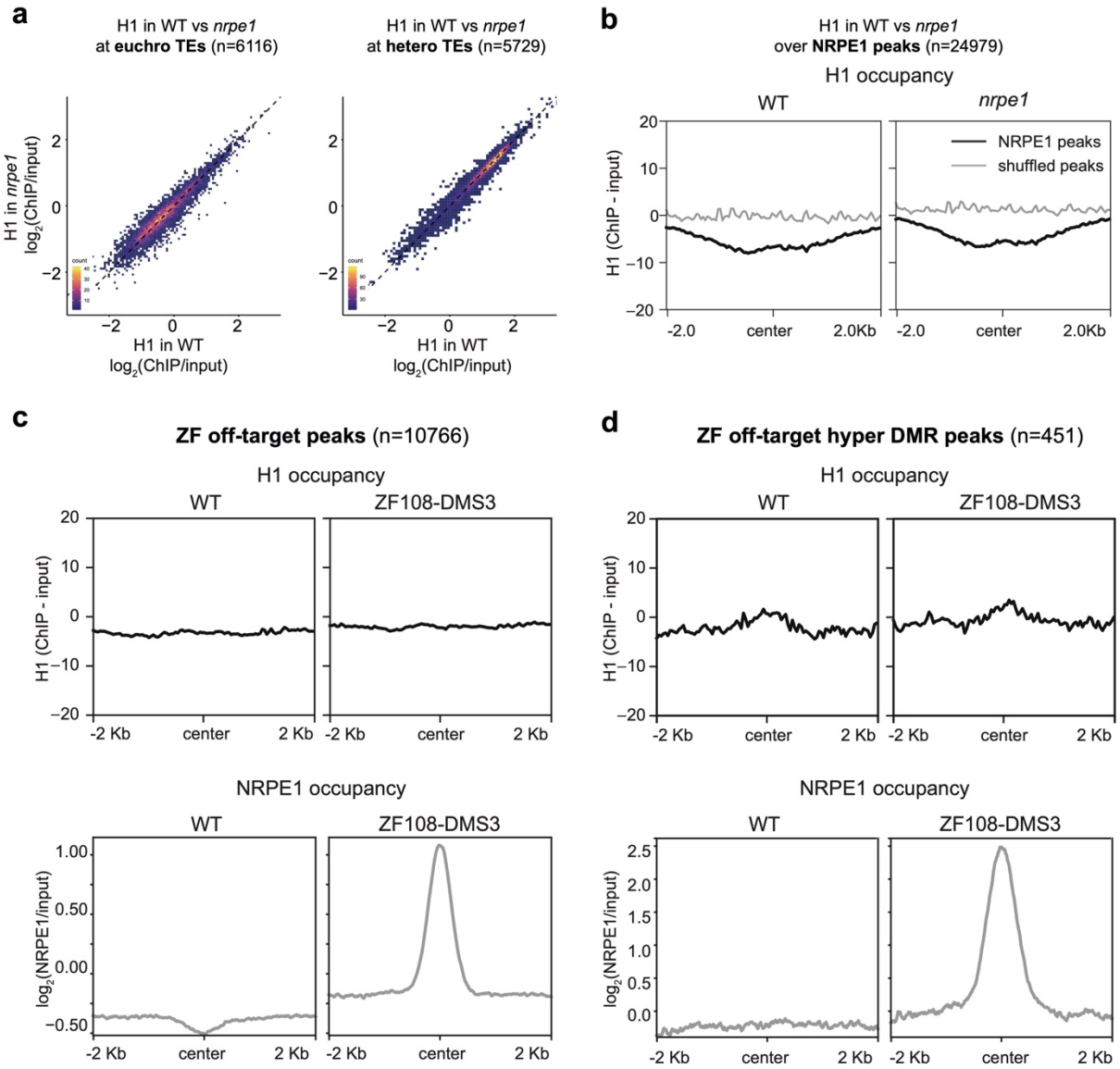

Figure 2 - RdDM does not reciprocally affect H1 localization: A) Scatter plot showing H1 enrichment in WT vs. *nrpe1* at euchromatic vs heterochromatic TEs. B) Metaplot showing H1 enrichment at NRPE1 peaks in WT vs. *nrpe1* C) H1 and NRPE1 occupancy at ZF-DMS3 off target peaks. Upper panel: H1 occupancy in WT vs. ZF108-DMS3. Lower panel: NRPE1 occupancy in WT vs. ZF108-DMS3. Chromatin from the same sample was used for both H1 and NRPE1 ChIP-seq data, so the lower panel serves as a control showing that ZF108-DMS3 is recruited to these off-target regions in these samples, despite H1 localisation remaining unchanged. D) Same as C) at the subset of regions where CHH methylation is gained in ZF108-DMS3 (Liu et al 2018), indicating that the fully functioning RdDM pathway is recruited to these regions.

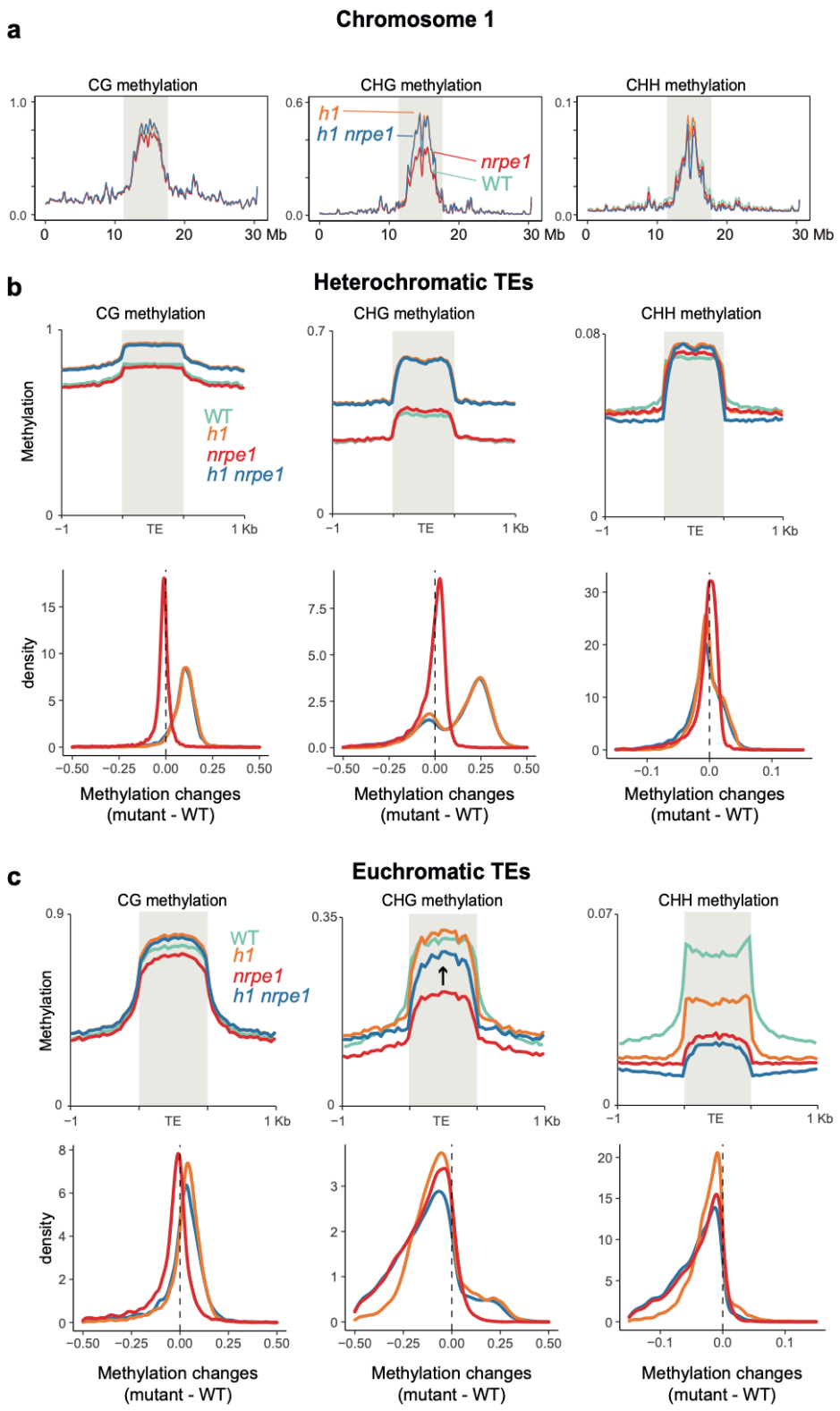
a
Chromosome 1
CG methylation
CHG methylation
CHH methylation
h1
h1 nrpe1
nrpe1
WT
30 Mb
b
Heterochromatic TEs
Methylation
WT
h1
nrpe1
h1 nrpe1
TE
1 Kb
density
Methylation changes
(mutant - WT)
c
Euchromatic TEs

574

Figure 3 - Major CG and CHG methylation gains in *h1* are independent of RdDM: A) Chromosomal view of DNA methylation levels (average of 10kb windows) in the genotypes indicated on chromosome 1. Y-axis indicates fraction methylation (0-1). B) Methylation level over heterochromatic TEs. Upper panel: methylation metaplots, Lower panel - kernel density plots. In the kernel density plots, the average methylation is calculated for each TE in both mutant and WT, then then the methylation difference is calculated. The plot shows the frequency density of TEs that gain/lose DNA methylation in the regions in the mutants indicated. C) Methylation level over euchromatic TEs. Upper panel: metaplots, Lower panel - kernel density plots (as above). Arrow highlights the gain in CHG methylation in the *h1/nrpe1* double mutant, as compared to *nrpe1* alone.

575

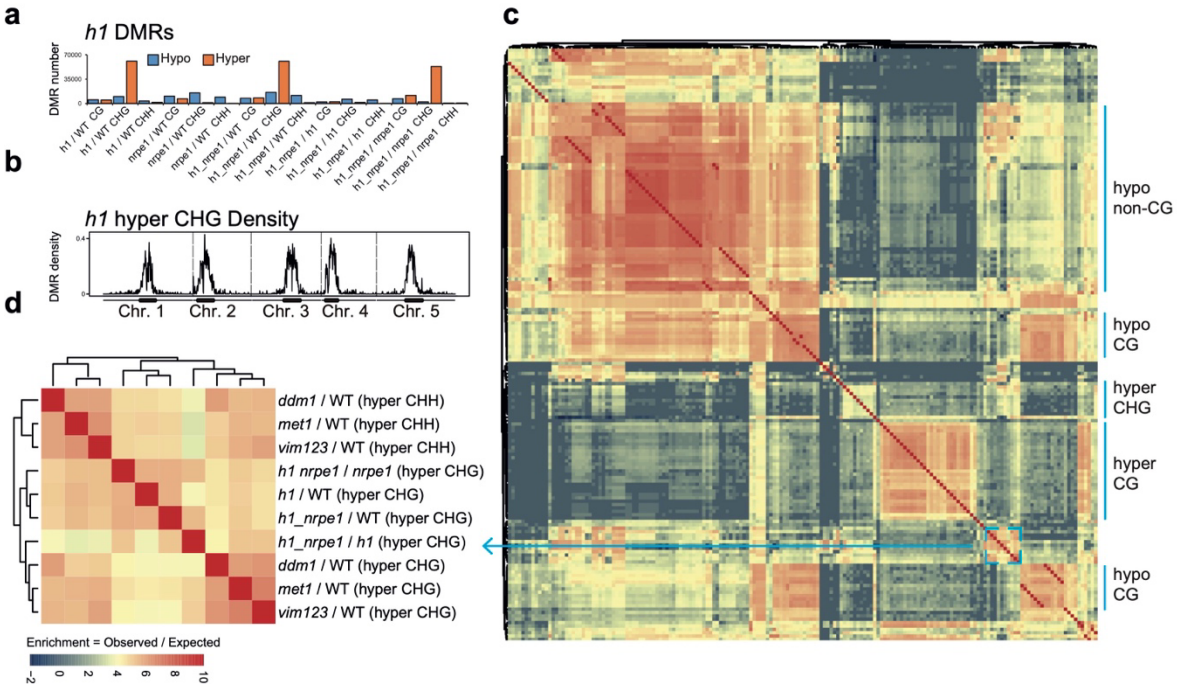

Figure 4 - Overlap analysis of *h1* hyper CHG DMRs with 96 methylation mutants: A) Number of hypo vs hyper DMRs in genotype comparisons indicated. B) *h1* hyper CHG DMR frequency density plot over Chromosomes 1-5. C) Similarity matrix based on pairwise overlapping scores (Co-Occurrence Statistics) of DMRs from 96 whole methylomes. . The labels on the right summarise the major functional categories of the methylation mutant genotypes in the cluster block. (individual genotypes are shown in Supplementary Figure 6). The colour scale represents the number of observed DMR overlaps between the pairwise comparison indicated over the number of overlaps expected by chance (DMRs randomly distributed throughout the genome). Red means highly enriched overlapping DMRs (similar genomic distribution), blue means highly non-overlapping (different genomic distribution) D) Zoomed in view of the cluster containing *h1* hyper CHG DMRs C) (see blue box and arrow).

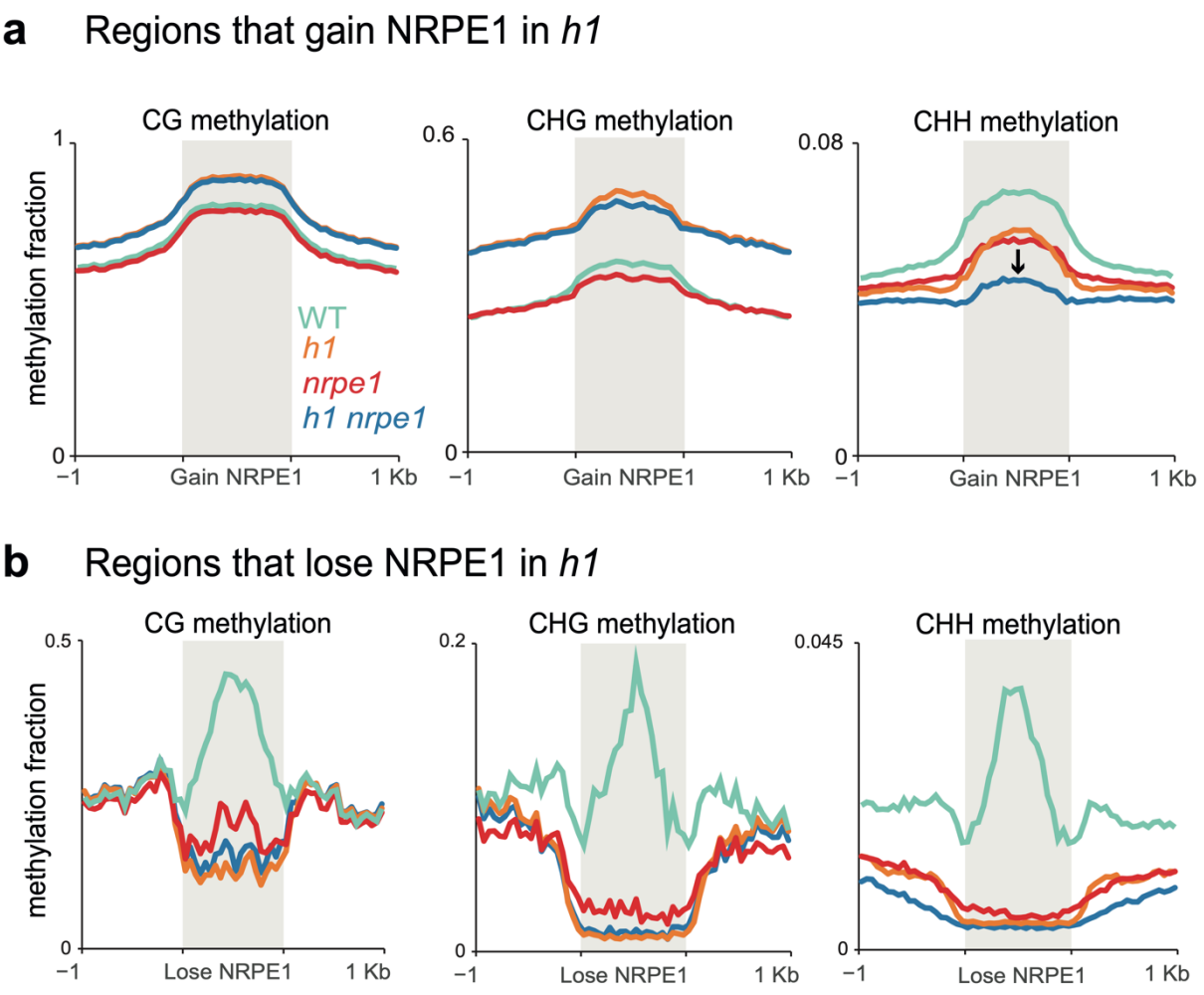

Figure 5 - Patterns of NRPE1 re-localisation in *h1* show corresponding methylation changes: A) Methylation metaplot in the genotypes indicated over regions of the genome that gain NRPE1 in *h1*. Arrow highlights the change in average CHH methylation in the *h1/nrpe1* double mutant as compared to the single mutants. B) Methylation metaplot of the genotypes indicated over regions of the genome that lose NRPE1 in *h1*.

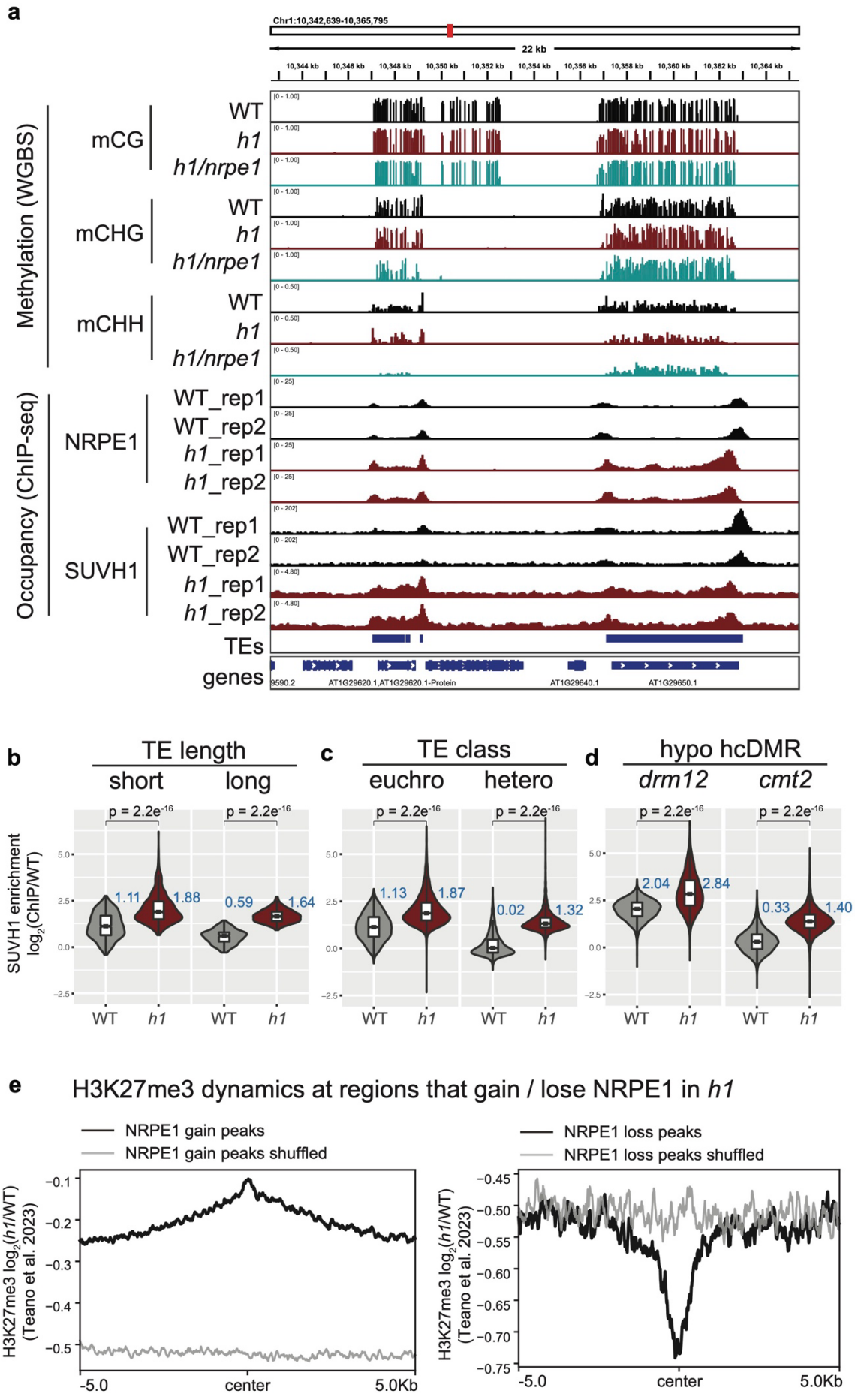
a
Chr1:10,342,639-10,365,795
22 kb
Methylation (WGBS)
mCG
mCHG
mCHH
WT
h1
h1/nrpe1
Occupancy (ChIP-seq)
NRPE1
SUVH1
WT_rep1
WT_rep2
h1_rep1
h1_rep2
TEs
genes
AT1G29620.1,AT1G29620.1-Protein
AT1G29640.1
AT1G29650.1
b
TE length
short
long
c
TE class
euchro
hetero
d
hypo hcDMR
drm12
cmt2
p = 2.2e-16
SUVH1 enrichment log2(ChIP/WT)
1.11
1.88
0.59
1.64
1.13
1.87
0.02
1.32
2.04
2.84
0.33
1.40
WT
h1
e
H3K27me3 dynamics at regions that gain / lose NRPE1 in h1
NRPE1 gain peaks
NRPE1 gain peaks shuffled
NRPE1 loss peaks
NRPE1 loss peaks shuffled
H3K27me3 log2(h1/WT) (Teano et al. 2023)
-5.0
center
5.0Kb

582

583

Figure 6 - SUVH1 encroaches heterochromatin in an *h1* mutant background: A) Genome browser image showing SUVH1 re-localisation in *h1* mirrors that of NRPE1. B-D) Boxplot inlaid violin plots showing SUVH1 enrichment in WT vs *h1* at short vs long TEs (B), at euchromatic vs heterochromatic TEs (C) and at drm12 vs cmt2 hypo CHH DMRs (D).